

# A catalog of early-type stars toward the Galactic center<sup>★ ★★</sup>

P. Grosbøl

European Southern Observatory, Karl-Schwarzschild-Str. 2, D-85748 Garching, Germany

Received ???; accepted ???

## ABSTRACT

**Context.** It is still unclear whether the Sagittarius spiral arm is a major spiral arm in the Galaxy or whether it just outlines a region of enhanced star formation because of the local compression of gas. The best way to separate these scenarios out is to study the kinematics across the arm to determine the velocity perturbation it induces.

**Aims.** A survey of early-type stars in the direction of the Galactic center is performed covering an area of 100 square degrees with the aim of identifying candidates for a radial velocity study.

**Methods.** Objective prism plates were obtained with the 4° prism on the ESO Schmidt telescope using IIaO, 4415, and IIIaJ emulsions. The plates were digitized and more than 100k spectra were extracted down to a limiting magnitude of  $B = 15^m$ . The spectra were cross-correlated with a template with Balmer lines, which yielded a candidate list of 12 675 early-type stars. Magnitudes and equivalent widths of strong lines were calculated from the spectra, which allowed us to estimate the individual extinctions and distances for 11 075 stars.

**Results.** The survey identified 9 571 candidate stars with a spectral type earlier than A1 and  $B < 14^m.5$  out to distances of more than 2 kpc, which is beyond the Sagittarius arm. This is indicated by the increase of absorption in the plane at distances larger than 0.5 kpc.

**Key words.** stars: early-type – ISM: dust, extinction – Galaxy: disk – Galaxy: stellar content – Galaxy: structure – surveys

## 1. Introduction

It is well known that young objects such as OB associations and HII-regions outline a four-armed spiral structure in the Galaxy (Georgelin & Georgelin 1976; Russeil et al. 2007; Vallée 2014; Reid et al. 2014). The dynamical nature of these arms is much less certain. In the case of the Sagittarius arm, two main scenarios are possible: that it is either i) a major spiral arm in the Galaxy with a significant mass (Drimmel 2000) associated with a spiral density wave (Lin & Shu 1964), or ii) a secondary gas compression, with increased star formation but little additional mass (Yáñez et al. 2008; Englmaier & Gerhard 1999). Whereas a direct estimate of the radial surface-density variation can be performed toward the Perseus arm (Monguió et al. 2015), a direct measurement of the stellar densities in the Sagittarius arm is very difficult owing to the heavy attenuation by dust toward the Galactic center. Another option for detecting a density enhancement in the arm is to observe the velocity variations of stars across it. The detection of a systematic radial velocity variation would strongly suggest the presence of a significant mass associated with the arm. However, the stellar population used for this type of study must be old enough to allow the stars to respond to a density perturbation (Wielen 1977). On the other hand, it should not be so old that its velocity dispersion has increased significantly since this would reduce its response and make a detection more difficult (Lin et al. 1969). An age range of 0.1–1 Gyr, corresponding to late B stars to early A stars, fulfills these criteria (Dehnen & Binney 1998). From a kinematic

point of view, the direction toward the Galactic center has the advantage of minimizing the influence of galactic rotation even though crowding is an issue.

The first step of such a kinematic study is to establish a reliable candidate list of early-type stars (e.g., B and A stars) toward the Galactic center. The high absorption by dust makes it impossible to obtain a reliable list using broadband visual colors. Although intermediate-band *uvby* photometry (Strömgren 1966) could be used, the lack of wide-field instruments with these filters in the Southern hemisphere excludes this option. Even near-infrared (NIR) wide-field surveys like 2MASS (Skrutskie et al. 2006) or VVV (Saito et al. 2012a,b), which are much less affected by extinction, cannot safely distinguish highly reddened early-type stars from late-type giants. An alternative is to use objective prism exposures with Schmidt telescopes, although overlapping spectra due to crowding is a concern. The presence of Balmer lines clearly identifies stars with spectral class F or earlier, even on low dispersion spectra. Furthermore, the strength of Balmer and Ca II lines allow us to break the ambiguity in estimating extinctions from stellar colors (Payne & Williams 1929).

The paper presents a search for early-type stars in the direction toward the Galactic center using objective prism plates. The next section describes the observations and basic reductions of the spectra, including astrometric calibrations. Synthetic photometry derived from the spectra and the fits to Balmer lines, if present, are presented in Sect. 2.2, whereas extinctions and distances for early-type stars are provided in Sect. 3. A comparison with major NIR surveys is given in Sect. 4. Finally, the spatial distribution of the early-type stars is shown in Sect. 5 while a general discussion of the sample and conclusions are provided in Sect. 6.

Send offprint requests to: P. Grosbøl, e-mail: pgrosbol@eso.org

★ Based on observations collected at the European Southern Observatory, La Silla, Chile (ESO programme 59.D-0143, 271.B-5007)

★★ The catalog of early-type stars is only available in electronic form at the CDS via anonymous ftp to cdsarc.u-strasbg.fr (130.79.128.5) or via <http://cdsweb.u-strasbg.fr/cgi-bin/qcat?J/A+A/>

## 2. Observations and reductions

All objective prism plates were obtained using the ESO 1m Schmidt telescope at La Silla with a scale of  $67.5'' \text{ mm}^{-1}$ . Its  $4^\circ$  prism was used, providing a nominal dispersion of  $45 \text{ nm mm}^{-1}$  at  $434 \text{ nm}$ . A first set of four plates were taken in 1977, with an exposure time of 8 min without filter using a IIa-O emulsion. The individual plates covered a  $5^\circ \times 5^\circ$  field. The spectra were widened to  $0.2 \text{ mm}$  on the plates which had a seeing in the range of  $2\text{--}3''$ . These plates were not used in the final analysis because of their coarse-grained emulsion, limited spectra range, and low sensitivity.

To overcome these issues, a second set of plates were taken at the ESO Schmidt in 1997, shortly before the telescope was decommissioned, using sensitized 4415 films and IIIa-J plates. The broad spectral sensitivity of these emulsions resulted in longer spectra which were not widened to reduce problems with overlaps. Both emulsions were developed in D-19 for  $5 \text{ min}$  at  $20^\circ \text{ C}$ . A full list of plates is given in Table 1.

All plates were digitized on the PDS 1010 microdensitometer at ESO in density mode. Owing to the limited size of the PDS stage, the plates were scanned in four parts of  $\sim 16 \text{ cm} \times 16 \text{ cm}$ , with a  $1 \text{ cm}$  overlap region. The plates were visually aligned so that the scan direction was along the dispersion. The actual alignment was measured on each scan and found to be better than  $0.3$  on average, except for the short, widened IIa-O spectra, where the error was around  $0.5$  with a maximum of  $1^\circ$ . The digitalization was made in a meander pattern with a speed of  $3 \text{ cm sec}^{-1}$ , which provided a correct recording of specular densities  $D < 3.0$  for a step function. The IIa-O plates were scanned with a squared aperture of  $20 \mu\text{m}$ , while  $10 \mu\text{m}$  was used for the finer-grained emulsions. With a step size equal to the aperture, this resulted in individual scans of  $8\text{k} \times 8\text{k}$  and  $16\text{k} \times 16\text{k}$  pixels, respectively. The density was set to zero on a part of the plate without emulsion while chemical fog,  $D_{\text{fog}}$ , was measured as the smallest density along the unexposed edge of the plates.

The ESO Schmidt did not provide a sensitometry wedge on the plates which made a direct measurement of the density-to-exposure relation impossible. To estimate the characteristic curve for the emulsions, five direct V-band exposures, which were centered on the plate fields, were obtained with the WFI CCD camera at 2.2m MPI/ESO telescope at La Silla. Even with a total exposure of 9 sec per field, the WFI/CCD frames were significantly deeper than the plates and reached  $V=17^m.5$  with errors of  $0^m.01$ . The WFI data were reduced with the ESO Image Survey pipeline (Nonino et al. 1999). The magnitudes of point sources on the reduced frames were estimated using SExtractor (Bertin & Arnouts 1996) and cross-identified with objects on the objective plates. The peak photographic density in the region between the  $H_\beta$  and  $H_\gamma$  lines were measured and plotted as a function of the V magnitudes, which yielded the characteristic curves for the emulsions. The formula by Sampson (1925) was used to compute relative intensities from densities

$$\log(I/I_0) = \gamma^{-1} \log(10^{(D-D_{\text{fog}})} - 1.0), \quad (1)$$

where  $\gamma$  is the photographic “contrast”. The main parameters for the characteristic curves are given in Table 2, where the number of stars used, the contrast, and saturation density  $D_s$  are listed. The inertia point  $V_{\text{ip}}$ , defined as the extrapolation of the linear part of the characteristic curve to zero density, is also given in V-band magnitudes.

Several early-type spectra were identified visually on the plates and averaged for each emulsion (see Fig. 1). Preliminary positions of candidate spectra were obtained by computing the

**Table 2.** Photographic contrast  $\gamma$ , inertia point  $V_{\text{ip}}$ , and saturation density  $D_s$  for emulsions. The offset  $\Delta_e$  of spectral cutoff relative to the  $H_\gamma$  line is also listed.

Emulsion	No.	Contrast $\gamma$	$V_{\text{ip}}$	$D_s$	$\Delta_e$ (mm)
IIa-O	94	$1.86 \pm 0.06$	$14^m.0$	3.0	1.023
4415	623	$2.66 \pm 0.08$	$15^m.7$	4.0	2.816
IIIa-J	126	$3.02 \pm 0.16$	$15^m.0$	3.9	1.640
IIIa-F	14	$2.07 \pm 0.38$	$17^m.4$	4.4	2.901

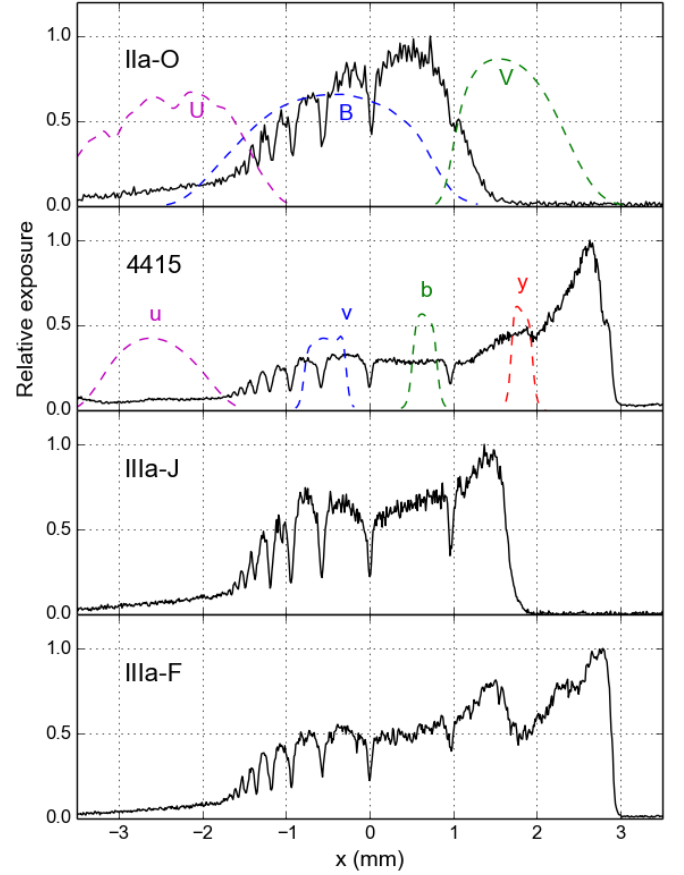


**Fig. 1.** Early-type template spectra for the 4 emulsions. The relative intensities of the spectra are plotted as a function of the linear distance from the  $H_\gamma$  line in the dispersion direction. For reference, passbands for the Bessel filters are over-plotted on the IIa-O plate, while Strömgren filters are shown on the 4415 spectrum.

linear correlation coefficient between the scans and the one-dimensional (1D) template spectra. The 4415 template was used for plate P13232 to match its spectral range. A selection threshold of 0.5 for the correlation coefficient gave initial candidate lists of 41 888, 135 413, and 99 027 spectra for the emulsions IIa-O, 4415 and IIIa-J, respectively. A search with SExtractor was also performed and yielded similar results, with many multiple detections along the spectra, however.

The extraction of 1D spectra from the scans was done by first analyzing a small rectangular region around each candidate position. The marginal distribution perpendicular to the dispersion, taking into consideration the tilt of the spectra measured for the scan, was computed and a search for peaks made. The spectrum was rejected as overlapping if several peaks were detected near

**Table 1.** List of Schmidt plates used.

Plate	RA <sub>2000</sub>	DEC <sub>2000</sub>	Start time	Exposure	Emulsion	Seeing	Remarks
P02310	17:35:26.3	-31:25:54	1977-09-16 18:35	8 <sup>m</sup>	IIa-O	2-3"	Spectra widened
P02311	17:35:24.8	-26:26:54	1977-09-16 19:06	8 <sup>m</sup>	IIa-O	2-3"	Spectra widened
P02312	17:55:26.6	-31:25:27	1977-09-16 19:28	8 <sup>m</sup>	IIa-O	2-3"	Spectra widened
P02313	17:55:25.0	-26:25:27	1977-09-16 19:50	8 <sup>m</sup>	IIa-O	2-3"	Spectra widened
P13133	17:46:53.7	-29:01:50	1997-04-11 07:25	5 <sup>m</sup>	4415	1.0"	Film, without prism
P13173	17:46:55.1	-31:06:25 <sup>a</sup>	1997-05-05 06:40	10 <sup>m</sup>	4415	0.9"	Film
P13174	17:36:41.6	-28:23:47 <sup>a</sup>	1997-05-05 07:10	10 <sup>m</sup>	4415	0.9"	Film
P13177	17:37:30.7	-33:44:00 <sup>a</sup>	1997-05-06 07:36	10 <sup>m</sup>	4415	1.6"	Film
P13178	17:57:15.8	-28:30:11 <sup>a</sup>	1997-05-06 08:00	10 <sup>m</sup>	4415	1.6"	Film
P13180	17:57:02.5	-33:29:33 <sup>a</sup>	1997-05-07 07:38	10 <sup>m</sup>	4415	0.9"	Film
P13225	17:37:25.9	-33:45:58 <sup>a</sup>	1997-08-27 00:08	10 <sup>m</sup>	IIIa-J	1.7"	
P13226	17:46:47.4	-31:08:27 <sup>a</sup>	1997-08-27 00:45	10 <sup>m</sup>	IIIa-J	1.7"	
P13231	17:36:33.9	-28:25:30 <sup>a</sup>	1997-08-28 23:41	10 <sup>m</sup>	IIIa-J	1.7"	
P13232	17:57:08.4	-28:31:35 <sup>a</sup>	1997-08-28 00:05	10 <sup>m</sup>	IIIa-J	1.7"	Likely a IIIa-F emulsion <sup>b</sup>
P13233	17:56:55.7	-33:30:59 <sup>a</sup>	1997-08-28 00:28	10 <sup>m</sup>	IIIa-J	1.8"	

**Notes.** <sup>(a)</sup> Telescope coordinates. The field is offset by 2° in declination because of the prism. <sup>(b)</sup> Although the plate envelop lists the emulsion as IIIa-J, both spectral range and photographic contrast suggest it is a IIIa-F plate.

to the main peak. The 1D spectra were extracted by converting densities to intensities using Eq. 1, subtracting nearby sky, and adding the intensities across the spectrum with the weights derived from the marginal distribution. The emulsions have a relative sharp spectral cutoff, which was easy to identify. The offsets between the cutoff, defined as the half intensity point, and the H<sub>γ</sub> lines was estimated from several early-type spectra. The average offset  $\Delta_e$  for each emulsion is given in Table 2. The spectra for which both H<sub>γ</sub> and H<sub>δ</sub>-lines had the expected location and a comparable equivalence width suggest that  $\Delta_e$  could be determined with an error of 22 $\mu$ , 9 $\mu$ , and 18 $\mu$  for the emulsions IIa-O, 4415 and IIIa-J, respectively. As reference position for the spectra, the location of the H<sub>γ</sub> line was used in the dispersion direction while the intensity weighted position was used perpendicular to it. For late-type spectra with no Balmer lines, the location of H<sub>γ</sub> was estimated using the offset  $\Delta_e$  derived for the emulsion type.

The dispersion relation for the plates was derived by fitting a 3<sup>rd</sup> order polynomial to the six Balmer line (i.e., H<sub>β</sub> to H<sub>9</sub>) that were identified on spectra of early-type stars. This gave a linear term of 45.61 nm mm<sup>-1</sup> at H<sub>γ</sub> with an error of 0.027 nm.

### 2.1. Astrometry

The brightest sources on each scan were visually cross-identified with the Tycho-2 Catalogue (Høg et al. 2000) to obtain astrometric calibrations that yield on average 50 matches. A linear transformation gave a standard deviation in the range of 2-4" and was used to find additional matches. An average of 200 stars in the Tycho-2 Catalogue (varying from 42 to 463 depending on the fields) was found to agree with the positions of the spectra within an error of 10". These stars were used for a full astrometric solution, which was done separately for right ascension and declination using five terms that include square and cross terms of X and Y coordinates. Pairs with residuals larger than 2.5" and 4.5" for right ascension and declination, respectively, were rejected leaving between 26 and 248 Tycho-2 stars per scan. The formal standard deviations for the transformations were around 0.5" for the 4415 emulsion in both coordinates, whereas the other emulsions had errors in the range 0.8-1.5" in declination as a result of their more shallow sensitivity cutoff.

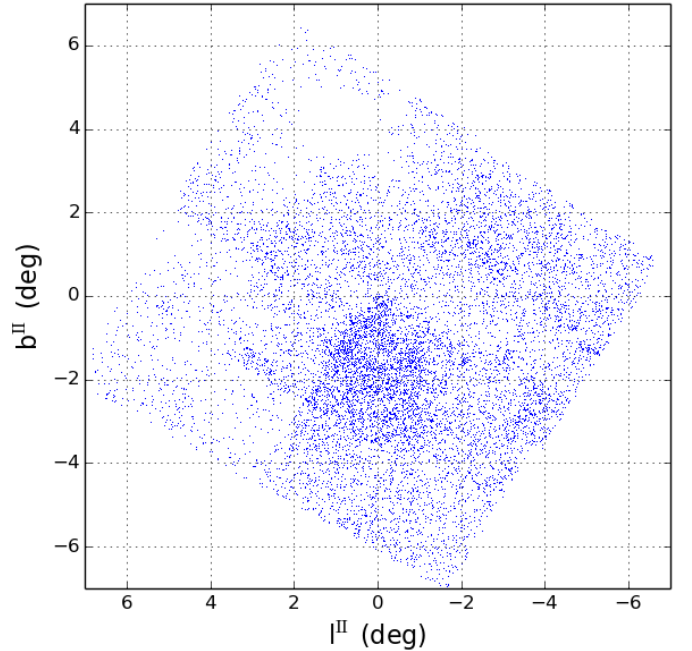


**Fig. 2.** The distribution of stars with Balmer lines on the P132 plates in galactic coordinates.

The actual astrometric errors are larger since the Tycho-2 stars are unevenly distributed on the scans and the transformations were extrapolated to the edges. An estimate of the maximum errors can be made by comparing the positions of stars located in the overlapping areas of different scans. The standard deviations of the differences for  $\alpha$  and  $\delta$  are given in Table A.1 and suggest that the error in right ascension is approximately 1", while declinations are determined to be better than 3" for the P131 plates and 6" for the other emulsions. Duplicate sources (i.e., spectra of the same source occurring on several scans or plates) were identified by matching their coordinates, magnitudes, and spectral gradient around H<sub>γ</sub>. The brightest of such duplicates was selected as the prime spectrum. In the case of the P132 plates, spectra on P13223 were given the lowest priority because of the uncertainty of the plate emulsion.

**Table 3.** Central wavelength, width, and ESO filter numbers for filters.

Filter	$\lambda_c$ (nm)	$\Delta\lambda$ (nm)	ESO filter
U <sub>b</sub>	354.0	53.7	ESO 602
B <sub>b</sub>	422.1	94.3	ESO 603
V <sub>b</sub>	542.1	104.8	ESO 606
u <sub>s</sub>	350.3	31.8	ESO 316
v <sub>s</sub>	412.4	19.4	ESO 317
b <sub>s</sub>	467.9	16.9	ESO 318
y <sub>s</sub>	548.6	21.6	ESO 319
Hbn	487.9	2.8	ESO 320
Hbw	487.9	15.3	ESO 321

**Table 4.** Astrometric and photometric uncertainties.

Plates quantity	P023		P131		P132	
	$\sigma$	n	$\sigma$	n	$\sigma$	n
m <sub>pg</sub>	0.06	5374	0.14	8910	0.25	5613
$\alpha$	0".9	5374	0".9	8910	1".1	5613
$\delta$	5".4	5374	1".6	8910	6".1	5613
B	0.17	296	0.25	285	0.23	136
(u-b)	0.17	25	0.15	13	0.08	7
c <sub>1</sub>	0.07	25	0.10	13	0.12	15
H <sub><math>\beta</math></sub>	-	-	0.03	4	-	-

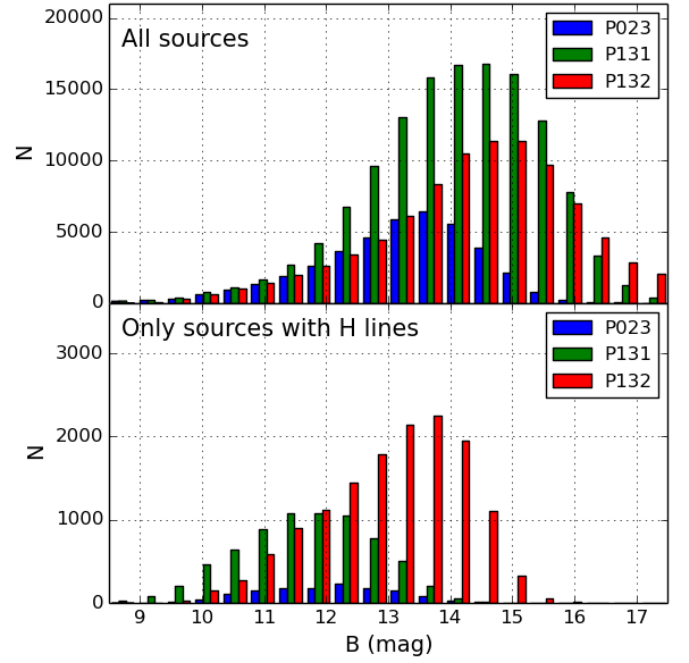
The distribution of spectra with Balmer lines are shown in galactic coordinate in Fig. 2 where a deficiency of stars in the regions of the Pipe Nebula around  $(l^{\text{II}}, b^{\text{II}}) = (1^\circ, 4^\circ)$  is clearly visible. It is also noted that plate P13232 is significantly shallower than the other plates in the P132 set.

## 2.2. Synthetic photometry

Synthetic photometry can be derived from the spectra since they were converted to relative intensities and their dispersion relation was estimated. Instrumental magnitudes were computed for several standard photometric bands using transmission curves for the Bessel broadband and Strömgren intermediate-band filters from the ESO filter list<sup>1</sup> as given in Table 3 and shown in Fig.1. The flux in each band was computed by converting its transmission curve into the linear scale of the objective prism spectra relative to H <sub>$\gamma$</sub> , correcting for the change in bin size, and convoluting it with the intensity along the spectra. Only the 4415 and IIIa-F emulsions cover the full wavelength range of all filters. Fluxes for V<sub>b</sub> and y<sub>s</sub> could not be computed for the other plates. The sensitivity cutoff of the emulsions was the primary spectral and positional reference for the sources. To improve the accuracy of the location of H <sub>$\gamma$</sub> , a template consisting of the Balmer lines H <sub>$\gamma$</sub>  through H <sub>$\epsilon$</sub>  was created and correlated with all spectra. For sources with a correlation peak larger than  $5\sigma$ , the H <sub>$\gamma$</sub>  line was refitted and used as wavelength reference.

The transformation to a standard system was done for the broadband colors using the Catalogue of Homogeneous Means in the UBV System (Mermilliod 1991) while the Strömgren filters were calibrated with the Catalogue of uvby-beta Data (Hauck & Mermilliod 1998). Although almost 500 UBV and 50 uvby measurements were found in these catalogs, crowding and saturation issues significantly limit the useful sample. All stars in clusters and with B<sub>J</sub>9<sup>m</sup> were excluded from the calibrations. Furthermore, the spectra were checked visu-

<sup>1</sup> see <http://filters.ls.eso.org/>


**Fig. 3.** Histograms of B magnitudes of sources for the three plate sets. Upper panel shows all sources while the lower one includes only sources with Balmer lines.

ally to remove stars with crowding issues. Errors and number of standards used are given in Table 4, while the coefficients of the linear transformation from standard to instrument system are listed in Table A.1. In addition to the synthetic photometry, Gaussian absorption line profiles were fitted to the H <sub>$\beta$</sub> (486.13nm), H <sub>$\gamma$</sub> (434.05nm), H <sub>$\delta$</sub> (410.17nm), H <sub>$\epsilon$</sub> (397.01nm), and Ca II K(393.37nm) lines from which their equivalent width (EW) was estimated. Spectra were classified as early-type (i.e., spectral class F or earlier) if their H <sub>$\gamma$</sub> , H <sub>$\delta$</sub> , and H <sub>$\epsilon$</sub>  lines were all significant at a  $3\sigma$  level and if their central wavelengths agreed within 0.5 nm. This gave 1 076, 6 116, and 12 675 early-type candidates for the plate sets P023, P131, and P132, respectively.

The distributions of B-magnitudes for sources on the three sets of plates are shown in Fig. 3. The P023 plates are the most shallow ones as expected. Although significantly more sources were found on the P131 plates than on the P132 set, the latter is almost one magnitude deeper than the former. This is caused by the high relative sensitivity in the red of the 4415 emulsion (see Fig.1), which favors the detection of nearby red dwarfs. The number of sources in the P023 and P132 samples agrees well above the limiting magnitude of the P023 plates which are nearly 2<sup>m</sup> shallower than the P132 set.

Internal errors of magnitudes were estimated based on the pixel-to-pixel noise along the spectra but were significantly smaller than external and systematic errors, such as variations of the characteristic curves as a function of wavelength, inhomogeneities across the plates, and contamination by nearby spectra. The limiting magnitude for the early-type sources on the P132 plates is B=13<sup>m</sup>.5 at a 95% completeness level, assuming a smoothly increasing source distribution.

## 3. Extinction and distances

The first step toward deriving physical parameters for stars is to estimate individual extinctions, which are expected to be



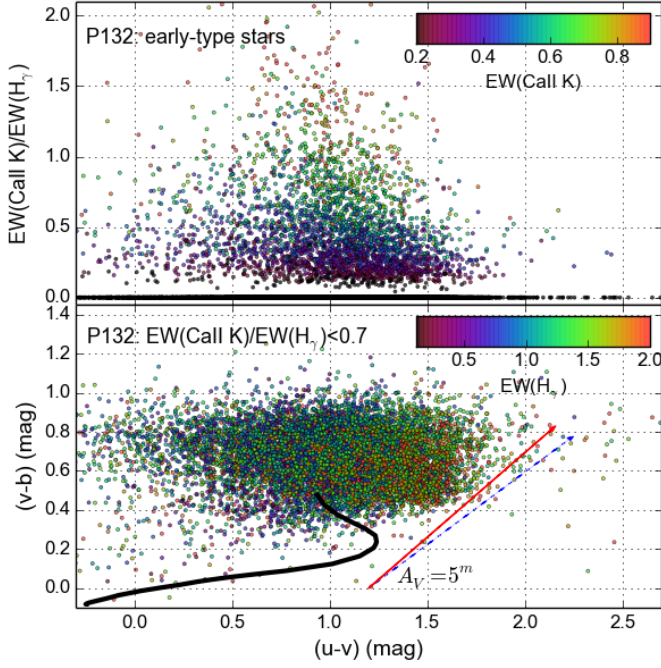


**Fig. 4.** Ratio of  $\text{EW}(\text{Ca II K})/\text{EW}(\text{H}_\gamma)$  and  $(v-b)$  as a function of  $(u-v)$  for early-type stars detected on the P132 plates. The thick line indicates the intrinsic colors of the stellar main-sequence. The two reddening vectors used are shown for  $A_V = 5^m$ .

significant towards the Galactic center. This was done on the P132 plates since they provide the faintest sample of early-type sources. Unfortunately, the IIIa-J emulsion does not cover the Strömgren  $y_s$ -band, making it impossible to use the reddening-independent Strömgren indices. Also the Bessel  $V_b$ -band is only partly within its sensitivity range, which leaves only combinations of the three bluest Strömgren filters. The two main options of color-color diagrams (CCD) are  $\text{Istr}$  vs.  $(u-b)$  and  $(v-b)$  vs.  $(u-v)$ , where the latter was preferred due to the higher photometric error in  $\text{Istr}$ . The standard problem of using these CCDs to estimate extinction is a local maximum in these indices which makes it difficult to distinguish between highly reddened early-type stars and less reddened late-type stars. This ambiguity can be resolved using the measured EWs of the Balmer and Ca II K lines. The presence of Balmer lines indicates that the star is earlier than G, while a significant Ca II K line places it later than A0 (i.e., the local maximum of the  $(u-v)$  index).

The  $(u-v)-(v-b)$  diagrams for early-type stars are shown in Fig. 4 for the P132 plates. The color relation for the intrinsic stellar “zero-age” main-sequence (ZAMS) was taken from the models by Marigo et al. (2008) using a 1 Myr isochrone with solar abundances. An isochrone with a metallicity  $Z=0.03$  was also used but yielded similar results for the early-type stars with effective temperatures in the range  $3.8 < \log(T_{\text{eff}}) < 4.5$  (i.e. with  $\text{EW}(\text{H}_\gamma) > 0.2 \text{ nm}$ ). The maximum values of  $(u-v)$  in this temperature range is 1.23 for  $\log(T_{\text{eff}}) = 3.96$ . The synthetic spectra by Munari et al. (2005) show that stars with this temperature have a ratio  $\text{EW}(\text{Ca II K})/\text{EW}(\text{H}_\gamma)$  of 0.7 which was subsequently used to distinguish which branch of the ZAMS to use for the estimate of extinctions. The color excesses for the indices are given by Schlegel et al. (1998) as  $E(v-b)/A_V = 0.152$  and  $E(u-v)/A_V = 0.205$ , while Schlafly & Finkbeiner (2011) estimate the excesses to be 0.162 and 0.187, respectively.

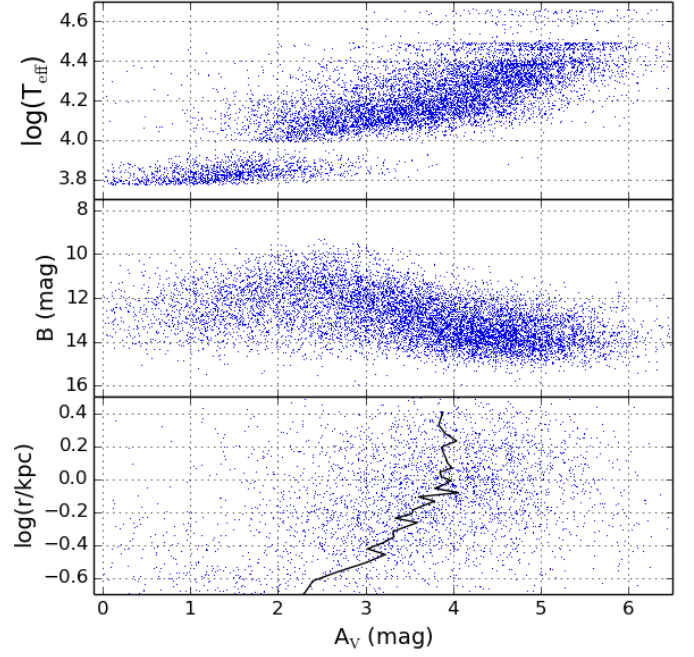


**Fig. 5.** Distributions of  $T_{\text{eff}}$ ,  $B$ , and distance  $r$  from the sun of early-type stars on the P132 plate set as a function of the visual extinction  $A_V$  estimated. The fully drawn line in the lower diagram represents the average values of  $A_V$ .

The stars in the CCD show a distribution that has the same general slope as the stellar ZAMS, but shifted by  $1-4^m$  of visual extinction. The bluest part has, on average, higher extinctions which is consistent with it containing intrinsic bright, early B-stars, which can be observed at larger distances. The color excesses by Schlafly & Finkbeiner (2011) were used since they yielded a larger number of stars, which is consistent with the intrinsic ZAMS. The distribution of stars with  $\text{EW}(\text{Ca II K})/\text{EW}(\text{H}_\gamma) > 0.7$  extends too far into the blue, possibly because of misidentified lines in the late A- and F-star spectra.

Visual extinctions  $A_V$  were only estimated for stars with colors that are consistent with them being reddened from the ZAMS, taking their  $\text{EW}(\text{Ca II K})$  into consideration, which yields a total of 9 571 stars earlier and 1 504 stars later than A1. Their  $T_{\text{eff}}$  were computed using the intrinsic  $(u-v)$  color of the isochrone. For B-type stars, the strength of the Balmer lines indicates the surface gravity  $g$  and can be used to correct absolute magnitude  $M_B$  for the stellar evolution above the ZAMS. The spectral models by Munari et al. (2005) were used to estimate the relation between  $\text{EW}(\text{H}_\delta)$ ,  $T_{\text{eff}}$ , and  $\log(g)$ .  $M_B$  was calculated by an interpolation in the ZAMS isochrone using  $T_{\text{eff}}$  and adding a correction that was dependent on  $\text{EW}(\text{H}_\delta)$  for B-stars. Finally, distances were calculated using  $A_B/A_V = 1.323$ .

The distribution of distances,  $B$ , and  $T_{\text{eff}}$  as functions of  $A_V$ , are given in Fig. 5. In a magnitude limit sample, hot bright stars can be observed at larger distances and higher extinctions than cooler stars, which yield a general correlation between  $A_V$  and  $T_{\text{eff}}$ . The deficiency of stars near A0 is caused by the local maximum in  $(u-v)$  where photometric errors spread sources to either side of the peak. Sources with low extinction (i.e.,  $A_V < 2^m$ ) are mostly cool, nearby stars and are evenly distributed in apparent magnitude within the limits of the sample. For higher extinction, an anti-correlation between  $B$  and  $A_V$  is seen, which is a

combined effect of the large volume surveyed and the high extinction.

For a given distance, the scatter in  $A_V$  is very significant, which reflects the patchy nature of the interstellar medium. The average extinction increases within the first kpc, while it is almost constant at greater distances. The latter is caused by a selection effect since only bright stars with relative low absorption can be observed. The photometric uncertainties in the (u-v) and (v-b) indices are  $\sim 0^m.15$ , which translates to an error  $\sigma_{A_V} = 0^m.3$ . Adding the uncertainty in B of  $\sigma_B = 0^m.23$ , the distance modulus has an error  $\sigma_{(m-M)} \approx 0^m.4$ , which corresponds to a relative error in distance of 20–30%.

#### 4. Comparison with the 2MASS survey

The high extinction in the direction of the Galactic center makes it interesting to cross-identify the sources found on the objective prism plates with NIR surveys since they are less affected by dust attenuation. The 2MASS catalog (Skrutskie et al. 2006) and the VVV survey (Saito et al. 2012a) are the most appropriate since their limiting magnitudes and area overlap match those of the current survey. A significant issue is the high density of stars toward the Galactic center, which makes an unambiguous identification difficult considering the astrometric uncertainties of the spectra (i.e., up to  $6''$  in  $\delta$ ). A more reliable identification can be obtained by matching spectra with Balmer lines only to early-type stars in the NIR surveys. Assuming the NIR color excesses used by Indebetouw et al. (2005), the reddening independent color index  $Q = (H-K) - 0.563*(J-H)$  was used to select early-type candidates with  $-0^m.05 < Q < 0^m.05$  corresponds to  $\log(T_{\text{eff}}) > 3.8$  according to the isochrone used above.

For the early-type stars on the P132 plates, 5 350 (45%) stars could be matched with 2MASS sources within  $\Delta(\alpha, \delta) = (3'', 16'')$  (i.e., three times their positional errors). The closest match was selected when multiple early-type candidates were found within the search area, which happened for 31% of the stars. The positional differences of the matches were  $\alpha_{\text{ops}} - \alpha_{2\text{MASS}} = 0^s.0 \pm 1^s.0$  and  $\delta_{\text{ops}} - \delta_{2\text{MASS}} = -4'.5 \pm 5'.9$ . A similar cross-identification was done with the VVV catalog although its first data release did not cover the full area. The VVV catalog contains many faint non-stellar sources which are much redder than stellar objects. This type of wrong cross-identifications were reduced by imposing a limit of  $K > 2.6 \times (J-K) + 14^m$  on matches. A total of 2 350 (35%) matches were found with  $\alpha_{\text{ops}} - \alpha_{\text{VVV}} = -0^s.0 \pm 1^s.5$  and  $\delta_{\text{ops}} - \delta_{\text{VVV}} = -0'.2 \pm 8'.6$ . The large errors in  $\delta$  were mainly located along the edges of the scans which indicates problems in the extrapolation of the astrometric solutions in this coordinate. A similar issue was not observed in  $\alpha$ .

The (J-K)–K and (J-K)–(U-B) diagrams for early-type sources on P132 that matched the NIR surveys are shown in Fig. 6, where average stellar colors and reddening vector are also plotted. The long tail of matches with  $0^m.5 < (J-K)$  and  $12^m < K$  are likely non-stellar sources erroneously associated with the stellar spectra. Most of these faint, non-stellar objects were identified on the VVV survey, which is significantly deeper than 2MASS. Because of saturation, many early-type sources are not matched with VVV.

In principle, extinctions can also be derived from the NIR data since  $\text{EW}(H_\gamma)$  can be used to avoid the confusion between reddened early-type stars and nearby late-type stars. Unfortunately, the color variation for early-type stars is too close to the reddening vector to make this feasible. Furthermore, wrong identifications yield a significant scatter.

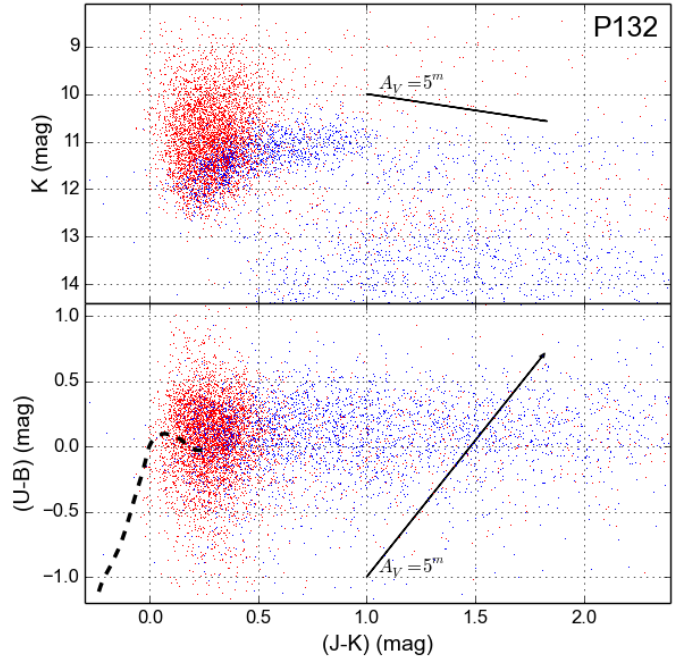


**Fig. 6.** Color-magnitude and color-color diagram of early-type sources detected on the P132 plates and cross-identified with 2MASS (red) and VVV (blue). The top panel shows the (J-K)–K diagram while (J-K)–(U-B) is displayed at the bottom. The main sequence for unreddened early-type stars is indicated by a black dashed line while the reddening vector is shown by an arrow.

#### 5. Properties of catalog

The distributions of the early-type stars on the P132 plates are shown in Fig. 7 as histograms that use a right-hand Cartesian coordinate system centered on the Sun, and with the x-axis pointed toward the Galactic center. A typical error bar is indicated on the figure corresponding to a relative error of 30% in distance at  $l^{\text{II}} = b^{\text{II}} = 2^{\circ}.5$ . The projection on the plane shows a smooth distribution, which is expected for a magnitude-limited sample, taking the survey area into consideration. More structure is seen perpendicular to the plane where a deficiency of stars in the plane is seen for distances larger than 0.5 kpc, likely associated with an increase in extinction in the Sagittarius arm.

The stellar densities of early-type stars in a cone of  $\pm 3^{\circ}$  around the Galactic center direction were computed as a function of  $x$  and  $z$  (see Fig 8). Cells of 10 pc were used perpendicular to the plane while a linear binning of 0.3 kpc was applied in the direction toward the Galactic center. The closest bin (i.e.,  $x=0.2-0.5$  kpc) shows an almost symmetric distribution with a centroid below the plane. All the more distant radial bins display significant dips (i.e.,  $> 5\sigma$ ) close to the plane associated with the extinction in the Sagittarius arm. All radial bins have a centroid below the plane that ranges from  $-10$  pc for  $x=0.5$  kpc to  $-22$  pc at a distance of 1.5 kpc, which is consistent with Joshi (2007).

#### 6. Discussion and conclusion

Of the three plate sets available, the P132 plates with IIIa-J emulsions turned out to be the best for detecting faint early-type stars in the direction of the Galactic center. More sources were found on the P131 films but most of them were red, late-type stars because of the high sensitivity in the red of the 4415 emulsions.

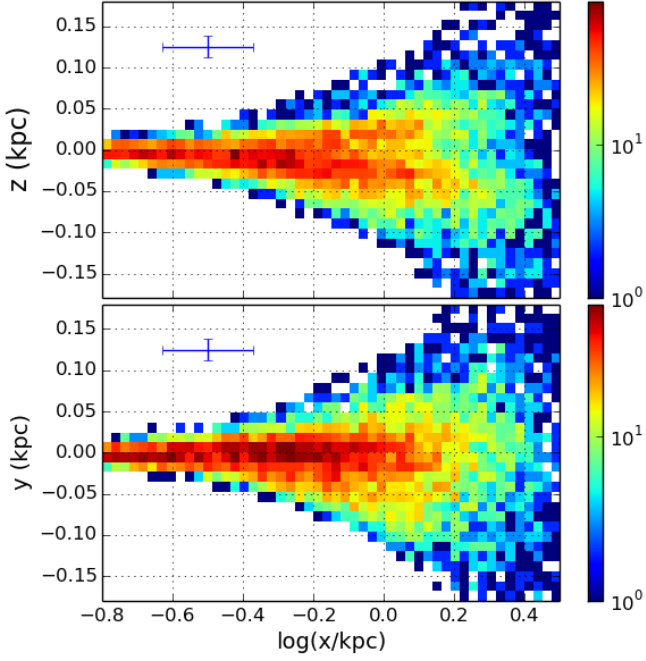


**Fig. 7.** Histograms of the spatial distribution of early-type stars on the P132 plates. The top plot shows the distribution perpendicular to the plane toward the Galactic center while the bottom diagram displays the histogram of stars in the Galactic plane. A typical error bar is shown for a distance error of 30% at  $l^{\text{II}} = b^{\text{II}} = 2.5$ .

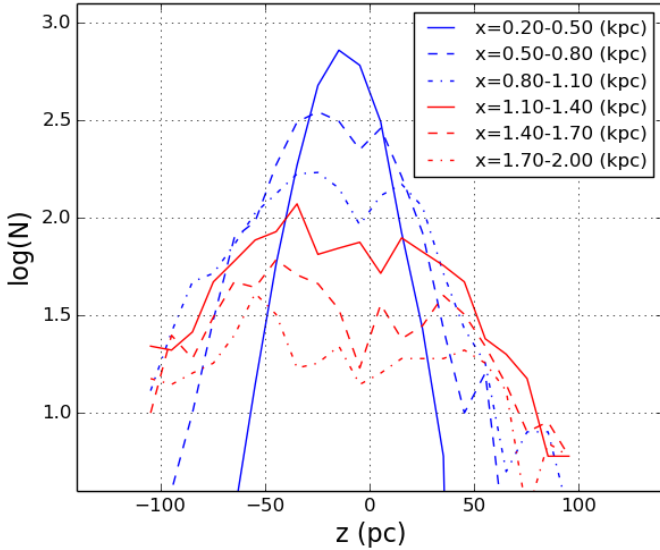


**Fig. 8.** Distribution of early-type stars on the P132 plates within a  $\pm 3^\circ$  cone around the direction to the Galactic center as a function of the height above the plane,  $z$ , and distance from the sun,  $x$ .

Furthermore, the long spectra on the P131 films made crowding a substantial issue. The old Iia-O were significantly shallower than the other two plate sets, because of both the emulsion and the widened spectra.

The spectra provide both general colors and EWs of the most prominent lines, which allow a reliable selection of early-type stars on the plates with 12675 candidates identified on the

P132 plate set. More importantly, the comparison of the EWs of Balmer lines and Ca II K enables a separation of stars that are hotter and cooler than A0 and, consequently, a resolution of the ambiguity in the estimate of individual extinctions using CCDs.

Although variable extinction and crowding make it impossible to evaluate a reliable volume density of stars as a function of distance, the survey area is large enough to obtain a reasonable sample of early-type stars toward the Galactic center. Assuming a smooth, intrinsic distribution function of the early-type stars, one can identify general features in the structure of the extinction. The most prominent is the increase of absorption in the Galactic plane which starts at a distance of 0.5-0.8 kpc from the sun and is associated with the Sagittarius arm, which is located at a Galactic centric distance of 6.6 kpc (Reid et al. 2014).

The increase of extinction in the plane suggests the presence of star formation associated with the Sagittarius spiral arm but does not indicate that a mass perturbation is associated with it. The safest way to decide if it is a major arm or not is to measure the velocity perturbation that is induced by the arm. The current survey of early-type stars has identified more than 9571 candidates earlier than A1 in the direction of the Galactic center at distances reaching beyond the Sagittarius arm. This sample can be used to study the kinematics of these stars as a function of distance and, thereby, to firmly determine the mass perturbation of the arm.

**Acknowledgements.** The main parts of the reductions were done with the ESO-MIDAS system while the analysis employed Python scripts that utilize the *scipy* library. This research made use of the SIMBAD database, operated at CDS, Strasbourg, France. This publication makes use of data products from the Two Micron All Sky Survey, which is a joint project of the University of Massachusetts and the Infrared Processing and Analysis Center/California Institute of Technology, funded by the National Aeronautics and Space Administration (NASA) and the National Science Foundation. Helpful comments by an anonymous referee were also appreciated.

## References

- Bertin, E. & Arnouts, S. 1996, A&AS, 117, 393
- Dehnen, W. & Binney, J. 1998, MNRAS, 298, 387
- Drimmel, R. 2000, A&A, 358, L13
- Englmaier, P. & Gerhard, O. 1999, MNRAS, 304, 512
- Georgelin, Y. M. & Georgelin, Y. P. 1976, A&A, 49, 57
- Hauck, B. & Merriliod, M. 1998, A&AS, 129, 431
- Høg, E., Fabricius, C., Makarov, V. V., et al. 2000, A&A, 355, L27
- Indebetouw, R., Mathis, J. S., Babler, B. L., et al. 2005, ApJ, 619, 931
- Joshi, Y. C. 2007, MNRAS, 378, 768
- Lin, C. C. & Shu, F. H. 1964, ApJ, 140, 646
- Lin, C. C., Yuan, C., & Shu, F. H. 1969, ApJ, 155, 721
- Marigo, P., Girardi, L., Bressan, A., et al. 2008, A&A, 482, 883
- Merriliod, J. C. 1991, Catalogue of Homogeneous Means in the UBV System, Tech. rep., Institut d'Astronomie, Université de Lausanne
- Mongiú, M., Grosbøl, P., & Figueras, F. 2015, A&A, 577, A142
- Munari, U., Sordo, R., Castelli, F., & Zwitter, T. 2005, A&A, 442, 1127
- Nonino, M., Bertin, E., da Costa, L., et al. 1999, A&AS, 137, 51
- Payne, C. & Williams, E. T. R. 1929, MNRAS, 89, 526
- Reid, M. J., Menten, K. M., Brunthaler, A., et al. 2014, ApJ, 783, 130
- Russeil, D., Adami, C., & Georgelin, Y. M. 2007, A&A, 470, 161
- Saito, R. K., Hempel, M., Minniti, D., et al. 2012a, A&A, 537, A107
- Saito, R. K., Minniti, D., Dias, B., et al. 2012b, A&A, 544, A147
- Sampson, R. A. 1925, MNRAS, 85, 212
- Schlafly, E. F. & Finkbeiner, D. P. 2011, ApJ, 737, 103
- Schlegel, D. J., Finkbeiner, D. P., & Davis, A. 1998, ApJ, 500, 525
- Skrutskie, M. F., Cutri, R. M., Stiening, R., et al. 2006, AJ, 131, 1163
- Strömgen, B. 1966, ARA&A, 4, 433
- Vallée, J. P. 2014, AJ, 148, 5
- Wielen, R. 1977, A&A, 60, 263
- Yáñez, M. A., Norman, M. L., Martos, M. A., & Hayes, J. C. 2008, ApJ, 672, 207

**Table B.1.** Column specifications for the table with data of early-type stars from P132 plate set.

Label	Format	Unit	Remarks
id_ops	A17	-	Identifier
RAdeg	D	deg	Right Ascension in J2000
DECdeg	D	deg	Declination in J2000
id_scan	A10	-	Scan identifier
Bmag	E	mag	Johnson B magnitude
U_Bj	E	mag	Johnson (U-B) index
u_vs	E	mag	Strömgren (u-v) index
v_bs	E	mag	Strömgren (v-b) index
Hg_ew	E	nm	Equivalent width of H <sub>γ</sub>
Hd_ew	E	nm	Equivalent width of H <sub>δ</sub>
He_ew	E	nm	Equivalent width of H <sub>ε</sub>
KCa_ew	E	nm	Equivalent width of Ca II K
Av	E	mag	Extinction in V
logTe	E	-	Logarithm of effective temperature
dBmag	E	mag	B magnitude above ZAMS
BMmag	E	mag	Absolute magnitude in Johnson B filter
dist	E	kpc	Distance from sun
start	E	um	Start of spectral scan relative to H <sub>γ</sub>
step	E	um	Step size of spectral scan
spec	1000E		Spectrum in relative intensities

## Appendix A: Photometric transformations

The photometric transformations from the standard system to observed magnitudes were estimated by linear least-square fits of the form

$$X_{\text{obs}} = c_X + a_X X_{\text{std}} \pm \sigma_X,$$

where  $X_{\text{std}}$  denotes the standard magnitude or color index, while  $X_{\text{obs}}$  is the observed values. The constant  $c_X$  and the linear term  $a_X$  are listed in Table A.1, where the root-mean-square of the fit  $\sigma_X$  and the number of sources used  $n_X$  are also given.

## Appendix B: Data table

The list of early-type stars on the P132 plate set is available through CDS<sup>1</sup> as a FITS table with the columns listed in Table B.1. Besides identifiers and coordinates, the synthetic photometry and equivalent width of main lines are provided. The original spectra scanned on the photographic plates are included in relative intensity units. The derived values for the individual extinctions and distances are also given. Tables for the other plate sets are available from the author.

<sup>1</sup> Centre de Données astronomiques de Strasbourg: <http://cds.u-strasbg.fr>



**Table A.1.** Photometric transformations.

Plates	$c_B$	$a_B$	$c_{(U-B)}$	$a_{(U-B)}$	$c_{(B-V)}$	$a_{(B-V)}$	$c_{(u-b)}$	$a_{(u-b)}$	$c_{c_1}$	$a_{c_1}$	$c_{H\beta}$	$a_{H\beta}$
	$\sigma_B$	$n_B$	$\sigma_{(U-B)}$	$n_{(U-B)}$	$\sigma_{(B-V)}$	$n_{(B-V)}$	$\sigma_{(u-b)}$	$n_{(u-b)}$	$\sigma_{c_1}$	$n_{c_1}$	$\sigma_{H\beta}$	$n_{H\beta}$
P023	-15.469	0.808	1.687	0.816	-	-	-0.406	1.016	-0.020	0.622	-	-
	0.173	296	0.132	261	-	-	0.174	25	0.068	25	-	-
P131	-16.428	0.918	1.529	0.753	0.096	1.297	-0.737	1.027	0.397	1.013	-0.727	1.026
	0.252	285	0.178	258	0.236	290	0.151	13	0.101	13	0.029	4
P132	-16.540	0.843	1.362	1.247	-1.071	0.812	-1.719	1.315	0.202	1.244	-	-
	0.234	136	0.175	122	0.243	136	0.076	7	0.119	15	-	-
P13232	-16.151	0.632	1.473	0.705	0.424	0.740	-0.578	0.823	0.257	1.387	-	-
	0.344	10	0.141	8	0.189	10	0.223	4	0.141	4	-	-